Published in final edited form as:
Curr Opin Neurobiol. 2012 February ; 22(1): 24–33. doi:10.1016/j.conb.2011.10.020.

Prospect for feedback guided surgery with ultra-short pulsed laser light

Diana Jeong[1,▯], **Philbert S. Tsai**[1,▯], and **David Kleinfeld**[1,2]

[1]Department of Physics, University of California at San Diego, La Jolla, CA

[2]Section of Neurobiology, University of California at San Diego, La Jolla, CA

Abstract

The controlled cutting of tissue with laser light is a natural technology to combine with automated stereotaxic surgery. A central challenge is to control the cutting of hard tissue, such as bone, without inducing damage to juxtaposed soft tissue, such as nerve and dura. We review past work that demonstrates the feasibility of such control through the use of ultrafast laser light to both cut and generate optical feedback signals via second harmonic generation and laser induced plasma spectra.

The anatomy of animals consists of a variety of distinct tissue types that may be directly juxtaposed to each other. Hard tissue constitutes bone in vertebrates and chitin in insects, while soft tissue constitutes skin, muscle, connective tissue, and nerve. The ability to surgically operate on hard tissue structures without inflicting damage to surrounding soft structures, such as removing bone while not affecting underlying nerve, is especially important for *in vivo* neurophysiological studies.

In vivo imaging of neuronal activity [1] or blood flow [2] in the brain with resolution near the optical diffraction limit typically requires mechanical thinning [3–5] or removal [6, 7] of a portion of the skull to gain optical access to the brain. The realization of a craniotomy or thinned-skull preparation requires fine surgical skill and is typically performed with a hand-held dental drill. The outcome of the procedure can vary widely from surgeon to surgeon. This influences the physiology of the underlying brain, including the potential for inflammation [8], disturbed vasodynamics [9], and cortical spreading depression [10]. Craniotomies often stand as the rate-limiting step in biomedical research that enables the use of sophisticated optical tools to image structures deep within the cortex [11, 12] of mouse models of brain function, in which structural or functional fluorescent indicators are expressed in specific cell types [13] (Fig. 1A). Lastly, a similar set of concerns exists for gaining optical access to the spinal cord [14].

Paths to automation of animal surgery are motivated by computer numerical control machine tools as a mechanism to guide a cutting tool to form craniotomies [15]. We consider the literature in support of ultra-short pulses of laser light, *i.e.*, of order 100

Correspondence: David Kleinfeld, Department of Physics 0374, University of California, 9500 Gilman Drive, La Jolla, CA 92093, Office: 858-822-0342, Fax: 858-534-7697, dk@physics.ucsd.edu.
▯equal contribution

femtosecond, as a tool for surgical cutting [16–23] (Fig. 1B). We then ask: (1) How can ultra-short pulses be incorporated with range-finding to provide constant control of the cutting path? (2) How can ultrashort pulses be combined with optical spectroscopy to provide feedback on the type of tissue being cut? (3) What are the prospects for an integrated surgical and diagnostic approach that can cut quickly and accurately, while minimizing collateral damage to neighboring tissue that must be preserved? This would allow plasma-mediated cutting to merge with robotic surgical techniques [24].

The physics of plasma-mediated ablation for cutting tissue

Plasma-mediated ablation with pulsed laser excitation builds on the concept of local excitation of molecules through nonlinear absorption, yet uses energy densities that are high enough to tear molecules apart rather than just drive electronic transitions that lead to fluorescent relaxation [25]. Energy fluence, defined as the energy per unit area in the pulse, is a natural metric to describe the extent of material damage produced by a short laser pulse focused to a spot. As an example, a 10-nJ, 100-fs pulse that is focused to an 1-μm^2 area yields a fluence of 1 J/cm^2 (Fig. 2) or an intensity of 10 TW/cm^2. This is equivalent to an electric field of ~ 10^8 V/cm or ~ 1 V/Å, which approaches the ~ 10 V/Å Coulomb field seen by valence electrons in atoms and molecules and leads to significant electron tunneling that frees bound electrons from their molecular orbitals [26].

The plasma grows as the free electrons seed an impact ionization cascade that involves acceleration of the electrons by inverse-Bremsstrahlung absorption, in which an electron absorbs photons while colliding with molecules [27]. After several absorption events, the free electrons achieve sufficiently high kinetic energy to ionize another molecule by impact ionization. This cascade, along with the continued generation of photoelectrons, leads to exponential growth of a micrometer-sized plasma bubble. Eventually the plasma becomes dense and limits the penetration of the incident light to a skin depth of only tens of nanometers. The restricted penetration depth provides axial localization of the plasma that is far less than the focal depth of the incident light.

The termination of the laser pulse is followed by recombination of the free electrons with the positively ionized molecules at the focus (Fig. 3A). This occurs on the picosecond time scale of electron collisions at typical electron densities and leads to a transfer of energy from the electrons to the material on a time scale that is short compared to the ~ 100 ps acoustic relaxation time in the material. The result is a dramatic pressure increase within the excitation volume that can produce a rupture of the material and form a cavitation bubble. The bubble constitutes the region of ablation. The expansion of the cavitation bubble is associated with an acoustic shockwave that propagates into the surrounding tissue [28] and has the potentially deleterious effect of spreading damage into the sample.

The special nature of plasma-mediated ablation with ultra-short pulses

The advantage of using ultra-short pulses, as opposed to nanosecond pulses, is a decrease in the threshold value of the fluence necessary to cause ablation [29–31] (Fig. 3B). The minimal fluence to achieve plasma-mediated ablation is of order 1 J/cm^2. In practice, fluences of 10 to 100 J/cm^2 have been used for the ablation of a number of hard tissues, beginning with pioneering work on cuticle [32], followed by the cutting of dental enamel [33], dentine [34] and, of direct relevance, bone [35–37] (Fig. 3C). The precision of plasma-mediated ablation of hard tissue was demonstrated by cutting microscopic features in bone [38] (Fig. 3D).

A critical issue for the use of plasma-mediated ablation in surgery is the magnitude and extent of the rise in temperature that surrounds the ablation region. The literature is

equivocal on this point. Theoretical calculations point to a rise in temperature that decays in less than a micrometer from the site of the plasma bubble [39]. Yet direct measurements of the rise in temperature range from one-tenth to ten degrees at distances of tens to hundreds of micrometers from the site of ablation [40–42]. As a practical matter, microscopic ablations have been achieved for the cutting of fine subcellular processes [43–48], as well as the cutting of corneal tissue [49, 50] and the manipulation of fine vascular processes [51–53]. Histological analyses of brain tissue ablated with a strongly focused beam show that the damage is confined to within a micrometer of the ablated surface [54] (Fig. 3E). *In toto*, these data support the utility of plasmamediated ablation with ultra-short laser pulses as a precision surgical tool.

Second harmonic generation for range-finding but not tissue identification

Automated surgery requires a means to detect the surface of the skull or other hard tissue as well as to map the local shape of the surface. Range-finding based on interferometric techniques is common, yet the range-finding can also be performed by harmonic generation with the ultra-short laser pulses [55]. In particular, second harmonic generation allows the front surface as well as the back surface of sufficiently thin materials to be mapped.

Second harmonic generation is a nonlinear process that produces coherent photons with twice the frequency of the incident laser pulses when the intensity of applied laser pulses is sufficiently high [56, 57]. The strength of the signal depends on the molecular structure of the material. It must be asymmetric, in the sense that opposing molecules do not point in opposite directions, and have a high second-order electric susceptibility. Many tissues, including bone [58, 59] (Fig. 4A) as well as connective tissue [60] (Fig. 4B), and nervous tissue [61] (Fig. 4C) meet these criteria. *In vivo* second harmonic imaging is particularly useful for feedback guided surgery since it depends only on intrinsic properties of the sample and does not require external dyes to image [62, 58, 63].

The second harmonic signal is diffraction limited and thus provides high spatial resolution as the beam is scanned through the sample. For scattering media, such as both hard and soft tissues, backscattered second harmonic signal from the surface and from the inside of the sample can be used for measuring the thickness [64–66]. The focus of the beam is scanned from above the surface of the sample and down along the z-axis [55] (Fig. 4D). The second harmonic signal will rise towards its maximum value as the focus enters the sample. It then drops in amplitude as the focus moves further into the sample where optical aberrations distort the focus of the beam and both incident and second harmonic photons are lost to scattering [55, 67–71] (Fig. 4E). The thickness of the sample can be determined from the intensity profile up to the depth that the second harmonic signal is undetectable; the maximum measureable thickness is likely to be less than 1 mm in analogy with the imaging depth of two photon laser scanning microscopy [72, 73].

Laser induced plasma spectroscopy for tissue identification

Second harmonic generation enables the non-disruptive determination of surface location and curvature and sample thickness, yet the signal is not unique to the type of tissue. The complementary technique of laser induced plasma spectroscopy [74–76] may be used to distinguish hard from soft tissue. Here, the light emitted from the ablation region (Fig. 3B), which corresponds to the recombination spectra of ionized atoms and molecules, is analyzed with a spectrometer to resolve the atomic composition of the material (Fig. 5A). The laser induced plasma spectrum can be used to distinguish biological samples based on their chemical composition [77–80]. In particular, bone and other calcified tissue may be distinguished from soft tissue based on the strong calcium emission peaks [81–83] (Fig. 5B).

Feedback guided surgery must frequently be performed in an aqueous environment to protect living tissue. In this case, the laser induced plasma spectrum may be unresolved as a result of pressure broadening and shortened emission lifetimes [84, 85]. A number of approaches have been implemented to overcome these complications. Of particular interest is the use of double-pulse excitation scheme [86–88, 83]. Here, the incident ultra-short laser pulse is split, with both pulses focused on the same region of the sample but with one delayed by order of one nanosecond relative to the other [89, 90]. The second pulse interacts with the plasma created by the first pulse and the emission spectrum has a greater signal-to-noise ratio than the spectrum after a single pulse. This improvement may relate to greater heating of the plasma, or the formation of an air-like expansion environment after the first pulse that minimizes pressure broadening of the plasma emission after the second pulse [91, 92, 86]. Further, temporal-gating of the collection of the spectra will isolate the signal from the initial broadband spectrum that is generated by nonlinear processes and initial pressure broadening at the center of the plasma bubble [93–95, 86, 76]. Details aside, the existing literature supports the real-time identification of bone versus soft tissue via their optical emission spectrum on a pulse by pulse basis (Fig. 5B) and forms the basis for control of the laser ablation beam.

Feasibility

An initial demonstration of feedback controlled surgery involved a perfused and fixed mouse head [96]. Plasma-mediated ablation with ultra-short laser pulses was used to cut an opening in the skull. The position of the head was under computer control via a three-axis motorized translation stage. The laser induced plasma spectrum was continuously monitored, with a scheme similar to that in Figure 5A, and was used to shutter the beam when regions of soft tissue were encountered. This led to a precision craniotomy that transversed the midline, a difficult manual procedure, without overt damage to the sagittal sinus (Fig. 6A). Range-finding was not incorporated in this demonstration.

The depth of the ablated region depends on the numerical aperture of the objective and the energy of the incident laser pulses [30, 31, 54]. Higher energy will lead to deeper cuts. Thus the full power of the amplified laser source cannot be utilized to make shallow cuts with a single focus near the interface of bone and soft tissue. Two schemes that can make complete use of the output of the amplified laser source are cutting with multiple foci, as an extension of multi-focal imaging techniques in two-photon laser scanning microscopy [97–100], and temporal focusing [101, 102]. The latter scheme utilizes the spectral bandwidth of the laser pulse to decouple the axial and lateral spatial widths of the focus, so that one can construct shallow, pancake-shaped foci whose axial extent is at the diffraction limit but whose lateral extent is broad. This technique was used to ablate a variety of materials, including skull [102] (Fig. 6B).

How rapidly can cutting be achieved? The most powerful commercial amplified system, currently the Wyvern™ 1000-30 Ti:Sapphire regenerative amplifier (Kapteyn-Murnane Laboratories, Inc., Boulder), produces 1.6 mJ pulses at 10 kHz. This implies an ablation rate of 1 mm^3 in 30 s for a single, temporally focused beam. The actual rate for removal of tissue can be faster if the ablation is designed to undercut the surface of the tissue. Lastly, temporal focusing may be further used to pattern as well as cut surfaces [103]; this may allow adhesives to stick more reliably to bone.

Epilog

No device currently exists that combines the cutting capability of plasmamediated ablation, using ultra-short laser pulses to ensure negligible collateral tissue damage, with feedback control of the cutting process. The techniques reviewed here for range-finding and online

tissue identification, all of which rely on the use of ultra-short pulses, can in principle be combined with plasmamediated ablation to achieve a device for automated removal of bone juxtaposed with soft tissues. This forms the basis of a tool to further industrialize experimental physiology [104] through the automatic realization of craniotomies and thinned skull transcranial windows (Fig. 1).

The challenges that abound for experimental studies in small animals are also present in numerous head and neck surgical procedures on human patients. Many surgical procedures with humans require thinning and removal of bone that overlies nerve and dura. As examples, these include procedures to decompress the optic, facial, or trigeminal nerve after tumor growth or traumatic injury as well as procedures to remove tumors from cranial regions that may be accessed through facial cavities, such as the *clivus*, a hollow that seats the pons, and the *sella turcica*, a hollow that seats the pituitary. Plasma-mediated ablation may prove to be useful for these tasks, where the relatively slow cutting rate of plasma-mediated ablation is offset by the precise feedback control.

Acknowledgments

We thank Joseph Neev for suggesting the possibility of feedback controlled surgery with ultra-short laser pulses, Christopher Bergeron for discussing potential applications to human surgical procedures, Jonathan Driscoll, Jeffrey Field, David Matthews and Jeffrey Moore for comments on a preliminary version of the article, and the National Institutes of Health for generous funding (EB003832).

References

1. Svoboda K, Denk W, Kleinfeld D, Tank DW. In vivo dendritic calcium dynamics in neocortical pyramidal neurons. Nature. 1997; 385:161–165. [PubMed: 8990119]
2. Kleinfeld D, Mitra PP, Helmchen F, Denk W. Fluctuations and stimulus-induced changes in blood flow observed in individual capillaries in layers 2 through 4 of rat neocortex. Proceedings of the National Academy of Sciences USA. 1998; 95:15741–15746.
3. Grutzendler J, Kasthuri N, Gan WB. Long-term dendritic spine stability in the adult cortex. Nature. 2002; 420:812–816. [PubMed: 12490949]
4. Drew PJ, Shih AY, Driscoll JD, Knutsen PM, Davalos D, Blinder P, Akassoglou K, Tsai PS, Kleinfeld D. Chronic optical access through a polished and reinforced thinned skull. Nature Methods. 2010; 7:981–984. [PubMed: 20966916]
5. Yang G, Pan F, Parkhurst CN, Grutzendler J, Gan WB. Thinned-skull cranial window technique for long-term imaging of the cortex in live mice. Nature Protocols. 2010; 5:201–208.
6. Levasseur JE, Wei EP, Raper AJ, Kontos AA, Patterson JL. Detailed description of a cranial window technique for acute and chronic experiments. Stroke. 1975; 6:308–317. [PubMed: 1154467]
7. Holtmaat A, Bonhoeffer T, Chow DK, Chuckowree J, De Paola V, Hofer SB, Hübener M, Keck T, Knott G, Lee WC, Mostany R, Mrsic-Flogel TD, Nedivi E, Portera-Cailliau C, Svoboda K, Trachtenberg JT, Wilbrecht L. Long-term, high-resolution imaging in the mouse neocortex through a chronic cranial window. Nature Protocols. 2009; 4:1128–1144.
8. Xu HT, Pan F, Yang G, Gan WB. Choice of cranial window type for in vivo imaging affects dendritic spine turnover in the cortex. Nature Neuroscience. 2007; 10:549–551.
9. Arieli A, Grinvald A, Slovin H. Dural substitute for long-term imaging of cortical activity in behaving monkeys and its clinical implications. Journal of Neuroscience Methods. 2002; 114:119–133. [PubMed: 11856563]
10. Piper RD, Lambert GA, Duckworth JW. Cortical blood flow changes during spreading depression in cats. American Journal of Physiology. 1991; 261:H96–H102. [PubMed: 1858935]
11. Helmchen F, Denk W. Deep tissue two-photon microscopy. Nature Methods. 2005; 2:932–940. [PubMed: 16299478]
12. Wilt BA, Burns LD, Wei Ho ET, Ghosh KK, Mukamel EA, Schnitzer MJ. Advances in light microscopy for neuroscience. Annual Review of Neurosciences. 2009; 32:435–506.

13. Miyawaki A. Innovations in the imaging of brain functions using fluorescent proteins. Neuron. 2005; 48:189–199. [PubMed: 16242400]

14. Davalos D, Lee JK, Smith WB, Brinkman B, Ellisman MH, Zheng B, Akassoglou K. Stable in vivo imaging of densely populated glia, axons and blood vessels in the mouse spinal cord using two-photon microscopy. Journal of Neuroscience Methods. 2008; 169:1–7. [PubMed: 18192022]

15. Pohl, MB.; Schumacher, A.; Hofmann, UG. Proceedings of the 5th International IEEE EMBS Conference on Neural Engineering. 2011. Towards an automated, minimal invasive, precision craniotomy on small animals.

16. Vogel A, Venugopalan V. Mechanisms of pulsed laser ablation of biological tissues. Chemical Reviews. 2003; 103:577–644. [PubMed: 12580643]

17. Mian SI, Shtein RM. Femtosecond laser-assisted corneal surgery. Current Opinion in Ophthalmology. 2007; 18(4):295–299. [PubMed: 17568205]

18. Ben-Yakar A, Bourgeois F. Ultrafast laser nanosurgery in microfluidics for genome-wide screenings. Current Opinion in Biotechnology. 2009; 20:100–105. [PubMed: 19278850]

19. Chung SH, Mazur E. Surgical applications of femtosecond lasers. Journal of Biophotonics. 2009; 2:557–572. [PubMed: 19606444]

20. Kohli V, Elezzabi AY. Prospects and developments in cell and embryo laser nanosurgery. Wiley Interdisciplinary Reviews of Nanomedicine and Nanobiotechnology. 2009; 1:11–25.

21. Soong HK, Malta JB. Femtosecond lasers in ophthalmology. American Journal of Ophthalmology. 2009; 147:189–197. [PubMed: 18930447]

22. Tsai PS, Blinder P, Migliori BJ, Neev J, Jin Y, Squier JA, Kleinfeld D. Plasma-mediated ablation: An optical tool for submicrometer surgery on neuronal and vascular systems. Current Opinion in Biotechnology. 2009; 20:90–99. [PubMed: 19269159]

23. Farid M, Steinert RF. Femtosecond laser-assisted corneal surgery. Current Opinion in Ophthalmology. 2010; 21:288–292. [PubMed: 20467316]

24. Lanfranco AR, Castellanos AE, Desai JP, Meyers WC. Robotic surgery: A current perspective. Annals of Surgery. 2004; 239:14–21. [PubMed: 14685095]

25•. Vogel A, Noack J, Huttman G, Paltauf G. Mechanisms of femtosecond laser nanosurgery of cells and tissues. Applied Physics B-Lasers and Optics. 2005; 81(8):1015–1047. This work presents a comprehensive review of the interaction of ultra-short pulsed laser light with living and fixed biological tissues.

26. Karplus, M.; Porter, RN. Atoms and Molecules: An Introduction for Students of Physical Chemistry. New York: W. A. Benjamin; 1970.

27. Joglekar AP, Liu HH, Meyhofer E, Mourou G, Hunt AJ. Optics at critical intensity: Applications to nanomorphing. Proceedings of the National Academy of Sciences USA. 2004; 101:5856–5861.

28. Schaffer CB, Nishimura N, Glezer EN, Kim AMT, Mazur E. Dynamics of femtosecond laser-induced breakdown in water from femtoseconds to microseconds. Optics Express. 2002; 10(3): 196–203. [PubMed: 19424350]

29. Stuart BC, Feit MD, Rubenchik AM, Shore BW, Perry MD. Laser-nduced damage in dielectrics with nanosecond to subpicosecond pulses. Physical Review Letters. 1995; 74:2248–2251. [PubMed: 10057880]

30. Loesel FH, Niemez MH, Bille JF, Juhasz T. Laser-induced optical breakdown on hard and soft tissues and its dependence on the pulse duration: Experiment and model. IEEE Journal of Quantum Electronics. 1996; 32:1717–1722.

31. Stuart BC, Feit MD, Herman S, Rubenchik AM, Shore BW, Perry MD. Nanosecond-to-femtosecond laser-induced breakdown in dielectrics. Physical Review B. 1996; 53:1749–1761.

32. Neev J, Nelson JS, Critelli M, McCullough JL, Cheung E, Carrasco WA, Rubenchik AM, Da Silva LB, Perry MD, Stuart BC. Ablation of human nail by pulsed lasers. Lasers in Surgery and Medicine. 1997; 21:186–192. [PubMed: 9261796]

33. Rode AV, Gamaly EG, Luther-Davies B, Taylor BT, Dawes J, Chan A, Lowe RM, Hannaford P. Subpicosecond laser ablation of dental enamel. Journal of Applied Physics. 2002; 92:2153–2158.

34. Weigl, P.; Kasenbacher, A.; Werelius, K. Femtosecond Technology for Technical and Medical Applications. Berlin: Springer-Verlag; 2004.

35. Armstrong WB, Neev JA, Da Silva LB, Rubenchik AM, Stuart BC. Ultrashort pulse laser ossicular ablation and stapedotomy in cadaveric bone. Lasers in Surgery and Medine. 2002; 30:216–220.

36. Schwab B, Hagner D, Bornemann J, Heermann R. The use of femtosecond technology in otosurgery. Topics in Applied Physics. 2004; 96:211–226.

37. Liu Y, Niemz M. Ablation of femural bone with femtosecond laser pulses: A feasibility study. Lasers in Medical Science. 2007; 22:171–174. [PubMed: 17242869]

38. Lim YC, Altman KJ, Farson DF, Flores KM. Micropillar fabrication on bovine cortical bone by direct-write femtosecond laser ablation. Journal of Biomedical Optics. 2009; 14 064021-1-10.

39. Stuart BC, Feit MD, Herman S, Rubenchik AM, Shore BW, Perry MD. Optical ablation by high-power short-pulse lasers. Journal of the Optical Society of America B. 1996; 13:459–468.

40. Ladieu F, Martin P, Guizard S. Measuring thermal effects in femtosecond laser-induced breakdown of dielectrics. Applied Physics Letters. 2002; 81:957–959.

41. Rode AV, Gamaly EG, Luther-Davies B. Subpicosecond laser ablation of dental enamel. Journal of Applied Physics. 2002; 92:2153–2158.

42. McCaughey RG, Sun H, Rothholtz VS, Juhasz T, Wong BJF. Femtosecond laser ablatiion of the stapes. Journal of Biomedical Optics. 2009; 14:0240401.

43. Tirlapur UK, Konig K. Targeted transfection by femtosecond laser light. Nature. 2002; 418:290–291. [PubMed: 12124612]

44. Heisterkamp A, Maxwell IZ, Mazur E, Underwood JM, Nickerson JA, Kumar S, Ingber DE. Pulse energy dependence of subcellular dissection by femtosecond laser pulses. Optics Express. 2005; 13:3690–3696. [PubMed: 16035172]

45. Shen N, Datta D, Schaffer CB, LeDuc P, Ingber DE, Mazur E. Ablation of cytoskeletal filaments and mitochondria in live cells using a femtosecond laser nanoscissor. Mechanical and Chemical Biosystems. 2005; 2:17–25.

46. Sacconi L, O'Connor RP, Jasaitis A, Masi A, Buffelli M, Pavone FS. In vivo multiphoton nanosurgery of cortical neurons. Journal of Biomedical Optics. 2007; 12:1–3.

47. Guo SX, Bourgeois F, Chokshi T, Durr NJ, Hilliard MA, Chronis N, Ben-Yakar A. Femtosecond laser nanoaxotomy lab-on-a chip for in vivo nerve regeneration studies. Nature Methods. 2008; 5:531–533. [PubMed: 18408725]

48. Nguyen J, Ferdman J, Zhao M, Huland D, Saqqa S, Ma J, Nishimura N, Schwartz TH, Schaffer CB. Sub-surface, micrometer-scale incisions produced in rodent cortex using tightly-focused femtosecond laser pulses. Laers in Surgery and Medicine. 2011; 43:382–391.

49. Soong HK, Mian S, Abbasi O, Juhasz T. Femtosecond laser-assisted posterior lamellar keratoplasty: Initial studies of surgical technique in eye bank eyes. Ophthalmology. 2005; 112:44–49. [PubMed: 15629819]

50. Binder PS, Sarayba M, Ignacio T, Juhasz T, Kurtz R. Characterization of submicrojoule femtosecond laser corneal tissue dissection. Journal of Cataract and Refractive Surgery. 2008; 34(1):146–152. [PubMed: 18165095]

51. Nishimura N, Schaffer CB, Friedman B, Tsai PS, Lyden PD, Kleinfeld D. Targeted insult to individual subsurface cortical blood vessels using ultrashort laser pulses: Three models of stroke. Nature Methods. 2006; 3:99–108. [PubMed: 16432519]

52. Nishimura N, Rosidi NL, Iadecola C, Schaffer CB. Limitations of collateral flow after occlusion of a single cortical penetrating arteriole. Journal of Cerebral Blood Flow and Metabolism. 2010; 30:1914–1927. [PubMed: 20842163]

53. Yalcin HC, Shekhar A, Nishimura N, Rane AA, Schaffer CB, Butcher JT. Two-photon microscopy-guided femtosecond-laser photoablation of avian cardiogenesis: Noninvasive creation of localized heart defects American. Journal of Physiology: Heart and Circulation Physiology. 2010; 299:H1728–1735.

54. Tsai PS, Friedman B, Ifarraguerri AI, Thompson BD, Lev-Ram V, Schaffer CB, Xiong Q, Tsien RY, Squier JA, Kleinfeld D. All-optical histology using ultrashort laser pulses. Neuron. 2003; 39:27–41. [PubMed: 12848930]

55•. Guo Y, Ho PP, Savage H, Harris D, Sacks P, Schantz S, Liu F, Zhadin N, Alfano RR. Second-harmonic tomography of tissues. Optics Letters. 1997; 22:1323–1325. This work introduces the

use of second harmonic generation as a tool for tomography of biological tissues. [PubMed: 18188227]

56. Shen, YR. The Principles of Nonlinear Optics. New York: John Wiley and Sons; 1984.
57. Boyd, RB. Nonlinear Optics. 2. Vol. 2003. Academic Press;
58. Zipfel WR, Williams RM, Christie R, Nikitin AY, Hyman BT, Webb WW. Live tissue intrinsic emission microscopy using multiphoton-excited native fluorescence and second harmonic generation. Proceedings of the National Academy of Sciences USA. 2003; 100:7075–7080.
59. Nadiarnykh O, Plotnikov S, Mohler WA, Kalajzic I, Redford-Badwal D, Campagnola PIJ. Second harmonic generation imaging microscopy studies of osteogenesis imperfecta. Journal of Biomedical Optics. 2007; 12:051805. [PubMed: 17994883]
60. Mohler WA, Millard AC, Campagnola PJ. Second harmonic generation imaging of endogenous structural proteins. Metholds. 2003; 29:97–109.
61. Dombeck DA, Kasischke KA, Vishwasrao HD, Ingelsson M, Hyman BT, Webb WW. Uniform polarity microtubule assemblies imaged in native brain tissue by second-harmonic generation microscopy. Proceedings of the National Academy of Sciences USA. 2003; 100:7081–7086.
62. Campagnola PJ, Clark HA, Mohler WA, Lewis A, Loew LM. Second-harmonic imaging microscopy of living cells. Journal of Biomedical Optics. 2001; 6:277–286. [PubMed: 11516317]
63. Mertz J. Nonlinear microscopy: New techniques and applications. Current Opinion in Neurobiology. 2004; 14:610–616. [PubMed: 15464895]
64. Mertz J, Moreaux L. Second-harmonic generation by focused excitation of inhomogeneously distributed scatterers. Optics Communications. 2001; 196:325–330.
65. Williams RM, Zipfel WR, Webb WW. Interpreting second-harmonic generation images of collagen I fibrils. Biophysical Journal. 2005; 88:1377–1386. [PubMed: 15533922]
66. Legare F, Pfeffer C, Olsen BR. The role of backscattering in SHG tissue imaging. Biophysical Journal. 2007; 93:1312–1320. [PubMed: 17449666]
67. Koenig K, Riemann I. High-resolution multiphoton tomography of human skin with subcellular spatial resolution and picosecond time resolution. Journal of Biomedical Optics. 2003; 8:432–439. [PubMed: 12880349]
68. Jiang Y, Tomov I, Wang YM, Chen ZP. Second-harmonic optical coherence tomography. Optics Letters. 2004; 29:1090–1092. [PubMed: 15181995]
69. Koehler MJ, Koenig K, Elsner P, Bueckle R, Kaatz M. In vivo assessment of human skin aging by multiphoton laser scanning tomography. Optics Letters. 2006; 31:2879–2881. [PubMed: 16969409]
70. Chu SW, Tai SP, Chan MC, Sun CK, Hsiao IC, Lin CH, Chen YC, Lin BL. Thickness dependence of optical second harmonic generation in collagen fibrils. Optics Express. 2007; 15:12005–12010. [PubMed: 19547564]
71. Koenig K. Clinical multiphoton tomography. Journal of Biophotonics. 2008; 1:13–23. [PubMed: 19343631]
72. Oheim M, Beaurepaire E, Chaigneau E, Mertz J, Charpak S. Two-photon microscopy in brain tissue: Parameters influencing the imaging depth. Journal of Neuroscience Methods. 2001; 111:29–37. [PubMed: 11574117]
73. Theer P, Denk W. On the fundamental imaging-depth limit in two-photon microscopy. Journal of the Americal Optical Society A. 2006; 23:3139–3150.
74. Margetic V, Pakulev A, Stockhaus A, Bolshov M, Niemax K, Hergenroder R. A comparison of nanosecond and femtosecond laser-induced plasma spectroscopy of brass samples. Spectrochimica Acta Part B – Atomic Spectroscopy. 2000; 55:1771–1785.
75. Cremers, DA.; Radziemski, LJ. Handbook of laser-induced breakdown spectroscopy. San Francisco: Wiley; 2006.
76•. Gurevich EL, Hergenroeder R. Femtosecond laser-induced breakdown spectroscopy: Physics, applications, and perspectives. Applied Spectroscopy. 2007; 61:233A–242A. This work presents a comprehensive review of the laser induced plasma spectroscopy.

77. Assion A, Wollenhaupt M, Haag L, Mayorov F, Sarpe-Tudoran C, Winter M, Kutschera U, Baumert T. Femtosecond laser-induced-breakdown spectrometry for Ca^{2+} analysis of biological samples with high spatial resolution. Applied Physics B Lasers and Optics. 2003; 77:391–397.

78. Corsi M, Cristoforetti G, Hidalgo M, Legnaioli S, Palleschi V, Salvetti A, Tognoni E, Vallebona C. Application of laser-induced breakdown spectroscopy technique to hair tissue mineral analysis. Applied Optics. 2003; 42:6133–6137. [PubMed: 14594075]

79. Samuels AC, DeLucia FC, McNesby KL, Miziolek AW. Laser-induced breakdown spectroscopy of bacterial spores, molds, pollens, and protein: Initial studies of discrimination potential. Applied Optics. 2003; 42:6205–6209. [PubMed: 14594086]

80. Trevizan LC, Freitas AZDE, Vieira ND. Evaluation of femtosecond laser-induced breakdown spectroscopy for analysis of animal tissues. Applied Spectroscopy. 2008; 62:1137–1143. [PubMed: 18926024]

81•. Kim BM, Feit MD, Rubenchik AM, Mammini BM, Da Silva LB. Optical feedback signal for ultrashort laser-pulse ablation of tissue. Applied Surface Science. 1998; 127:857–862. This work introduces laser induced plasma spectroscopy as a tool to distinguish hard tissue from soft tissue.

82. Samek O, Beddows DCS, Telle HH, Kaiser J, Liska M, Caceres JO, Urena AG. Quantitative laser-induced breakdown spectroscopy analysis of calcified tissue samples Spectrochimica. Acta Part B – Atomic Spectroscopy. 2001; 56:865–875.

83. Abdel-Salam ZA, Nanjing Z, Anglos D, Harith MA. Effect of experimental conditions on surface hardness measurements of calcified tissues via LIBS. Applied Physics B – Lasers and Optics. 2009; 94:141–147.

84. Cremers DA, Radziemski LJ, Loree TR. Spectrochemical analysis of liquids using the laser spark. Applied Spectroscopy. 1984; 38(5):721–729.

85. Pichahchy AE, Cremers DA, Ferris MJ. Elemental analysis of metals under water using laser-induced breakdown spectroscopy. Spectrochimica Acta Part B -Atomic Spectroscopy. 1997; 52:25–39.

86. De Giacomo A, Dell'Aglio M, De Pascale O, Capitelli M. From single pulse to double pulse ns-laser induced breakdown spectroscopy under water: Elemental analysis of aqueous solutions and submerged solid samples. Spectrochimica Acta Part B – Atomic Spectroscopy. 2007; 62:721–738.

87. Gottfried JL, De Lucia FC, Munson CA, Miziolek AW. Double-pulse standoff laser-induced breakdown spectroscopy for versatile hazardous materials detection. Spectrochimica Acta Part B – Atomic Spectroscopy. 2007; 62:1405–1411.

88. Lazic V, Colao F, Fantoni R, Spizzichino V, Jovicevic S. Underwater sediment analyses by laser induced breakdown spectroscopy and calibration procedure for fluctuating plasma parameters. Spectrochimica Acta Part B – Atomic Spectroscopy. 2007; 62:30–39.

89. Schiffem JT, Doerr DW, Alexander DR. Optimization of collinear double-pulse femtosecond laser-induced breakdown spectroscopy of silicon. Spectrochimica Acta Part B – Atomic Spectroscopy. 2007; 62:1412–1418.

90. Pinon V, Fotakis C, Nicolas G, Angios D. Double pulse laser-induced breakdown spectroscopy with femtosecond laser pulses. Spectrochimica Acta Part B-Atomic Spectroscopy. 2008; 63:1006–1010.

91. Yalcin S, Tsui YY, Fedosejevs R. Pressure dependence of emission intensity in femtosecond laser-induced breakdown spectroscopy. Journal of Analytical Atomic Spectrometry. 2004; 19:1295–1301.

92. Scaffidi J, Angel SM, Cremers DA. Emission enhancement mechanisms in dual-pulse LIBS. Analytical Chemistry. 2006; 78:24–32. [PubMed: 16419334]

93. Radziemski LJ, Loree TR, Cremers DA, Hoffman NM. Time-resolved laser-induced breakdown spectrometry of aerosols. Analytical Chemistry. 1983; 55:1246–1252.

94. Le Drogoff B, Margot J, Chaker M, Sabsabi M, Barthelemy O, Johnston TW, Laville S, Vidal F, von Kaenel Y. Temporal characterization of femtosecond laser pulses induced plasma for spectrochemical analysis of aluminum alloys. Spectrochimica Acta Part B – Atomic Spectroscopy. 2001; 56:987–1002.

95. Sirven JB, Bousquet B, Canioni L, Sarger L. Time-resolved and time-integrated single-shot laser-induced plasma experiments using nanosecond and femtosecond laser pulses. Spectrochimica Acta Part B – Atomic Spectroscopy. 6; 200459:1033–1039.

96. Jeong, D.; Tsai, PS.; Schafer, D.; Squier, J.; Neev, J.; Kleinfeld, D. Society for Neuroscience Annual Meeting. Society for Neuroscience; San Diego: 2010. All optical cranial surgery: Ablation of hard but not soft tissue by amplified femtosecond laser pulses and feedback from atomic emission spectra; p. 615.23/00041

97. Fittinghoff DN, Schaffer CB, Mazur E, Squier JA. Time-decorrelated multifocal micromachining and trapping. IEEE Journal of Selected Topics in Quantum Electronics. 2001; 7:559–566.

98. Carriles R, Sheetz KE, Hoover EE, Squier JA, Barzda V. Simultaneous multifocal, multiphoton, photon counting microscopy. Optics Express. 2008; 16:10364–10371. [PubMed: 18607447]

99. Sheetz KE, Hoover EE, Carriles R, Kleinfeld D, Squier JA. Advancing multifocal nonlinear microscopy: Development and application of a novel multibeam Yb:KGd(WO4)2 oscillator. Optics Express. 2008; 16:17574–17584. [PubMed: 18958037]

100. Cheng A, Gonçalves JT, Golshani P, Arisaka K, Portera-Cailliau C. Simultaneous two-photon calcium imaging at different depths with spatiotemporal multiplexing. Nature Methods. 2011; 8:139–142. [PubMed: 21217749]

101. Oron D, Silberberg Y. Spatiotemporal coherent control using shaped, temporally focused pulses. Optics Express. 2005; 13:9903–9908. [PubMed: 19503200]

102•. Vitek DN, Adams DE, Johnson A, Tsai PS, Backus S, Durfee CG, Kleinfeld D, Squier JA. Temporally focused femtosecond laser pulses for low numerical aperture micromachining through optically transparent materials. Optics Express. 2010; 18:8086–18094. This work introduces the application of temporally focused femtosecond laser pulses for efficient micromachining of bone.

103. Vitek DN, E Block E, Bellouard Y, Adams DE, Backus S, Kleinfeld D, Durfee CG, Squier JA. Spatio-temporally focused femtosecond laser pulses for nonreciprocal writing in optically transparent materials. Optics Express. 2010; 18:24673–24678. [PubMed: 21164813]

104. Kleinfeld D, Griesbeck O. From art to engineering? The rise of in vivo mammalian electrophysiology via genetically targeted labeling and nonlinear imaging. Public Library of Science Biology. 2005; 3:1685–1689.

105. Schaffer CB, Brodeur A, Mazur E. Laser-induced breakdown and damage in bulk transparent materials induced by tightly-focused femtosecond laser pulses. Measurement Science and Technology. 2001; 12:1784–1794.

Highlights

- Realization of a cranial window for *in vivo* imaging in rodents in a rate-limiting step in the surgical preparation.
- Plasma mediated ablation by ultra-short laser pulses provides a means to automate surgical cutting.
- Guidance for positioning of the cut can utilize second harmonic generation.
- Feedback for tissue identification, *i.e.*, to bone versus dura or brain, can utilize laser induced plasma spectroscopy.

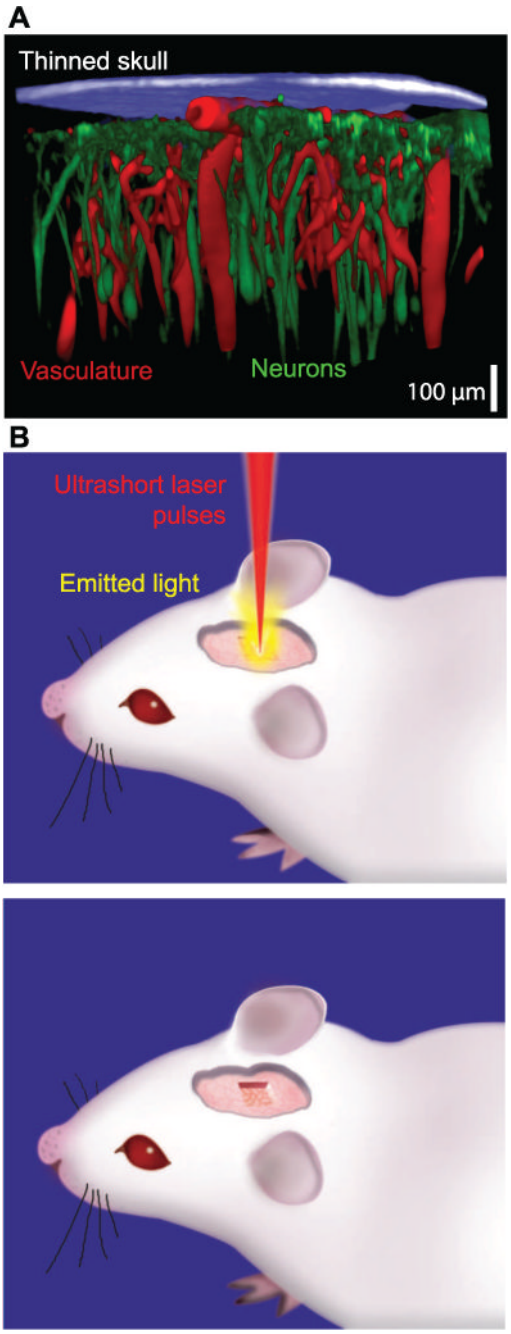

Figure 1. Cranial window to image brain function

(A) Maximal projection of a stack of images taken through a transcranial, thinned skull preparation. The skull was imaged with second harmonic generation (blue), the vasculature by two-photon laser scanning microscopy of blood plasma stained with the dye Texas red conjugated to dextran (70kDa) (red), and the pyramidal neurons of layer 5b were imaged via their endogenous expression of green fluorescent protein (green). Adapted from [4]. **(B)** Idealized schematic of the use of pulsed laser light to reliably cut away bone and form a craniotomy.

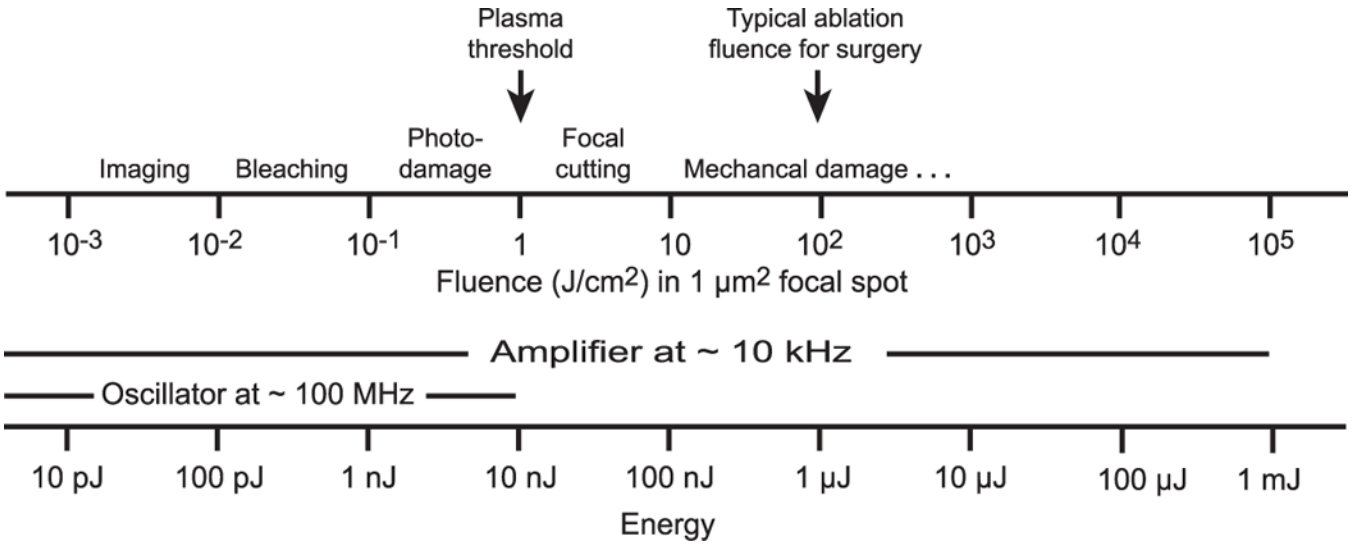

Figure 2. Scales in optical-assisted plasma-mediated ablation

A typical state-of-the-art amplified Ti:Sapphire system produces a 10 kHz train of 100 μJ 100-fs pulses, to achieve a peak power of 1 GW at an average power of 1 W.

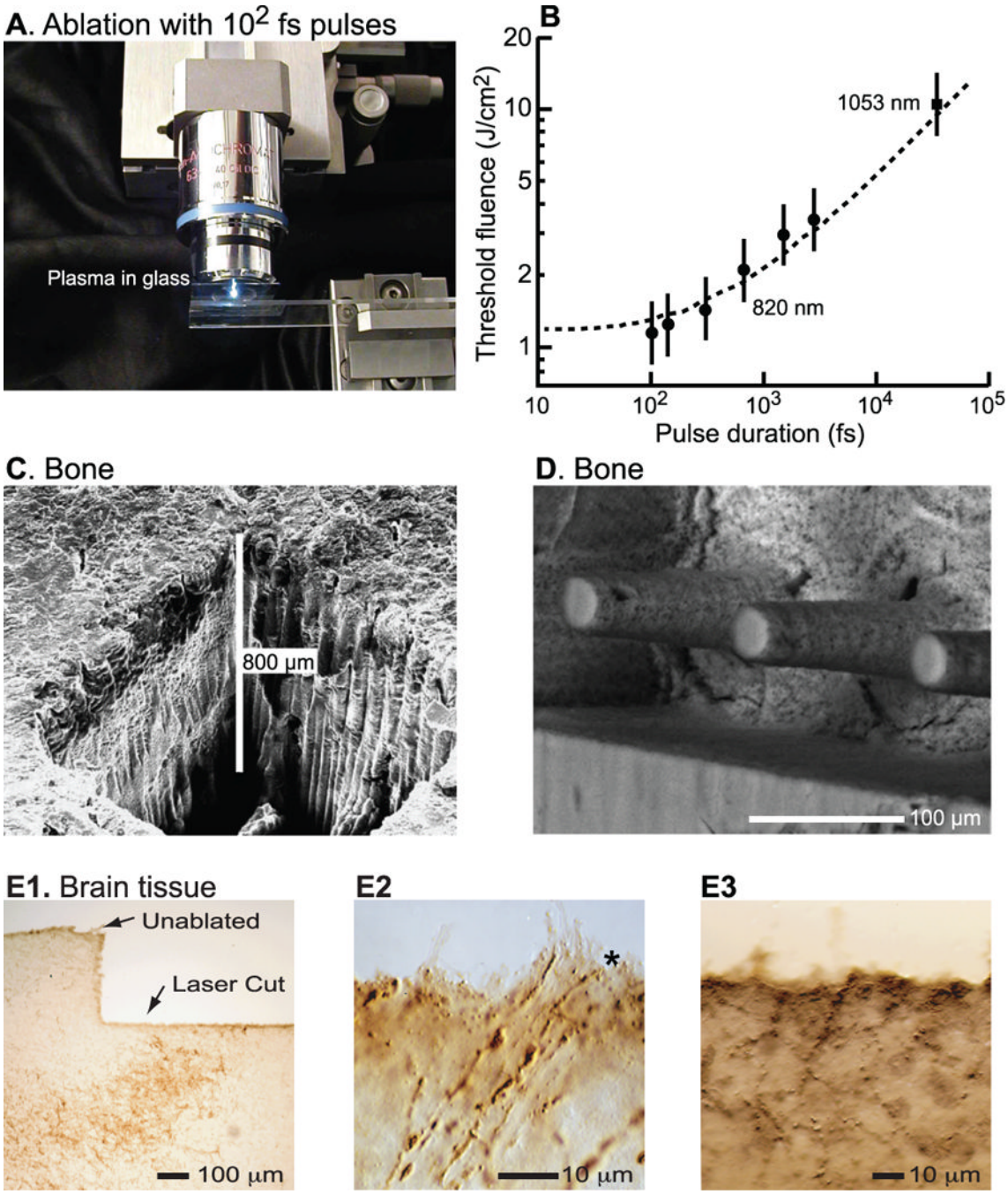

Figure 3. Plasma-mediated ablation of biological tissue with ultra-short laser pulses

(A) Emitted light from the plasma bubble in glass melted by 100-fs pulses whose fluence is well above threshold. Adapted from [105]. **(B)** Plot of minimum fluence for ablation as a function of pulse width. The short 100 fs pulses have the minimum fluence. Adapted from [30]. **(C)** Scanning electron micrograph of a procine long bone cut in air. Adapted from [37]. (**D)** Scanning electron micrograph of patterned bone cut in air. Adapted from [38]. **(E1)** Bright-field image of immunostained surface of fresh brain tissue from rat, cut under saline. After completion of the optical ablation, the tissue was fixed, frozen, physically sectioned at a thickness of 25 μm, immunostained with anti-tyrosine hydroxylase, and visualized with

diaminobenzadine precipitation. The brown regions correspond to immunostained axons and cell bodies. **(E2)** Tissue similar to that in panel G but imaged at high magnification to illustrate the cutting of individual axons (*). **(E3)** Immunoreactivity near an optically cut surface in unfixed neuronal tissue.

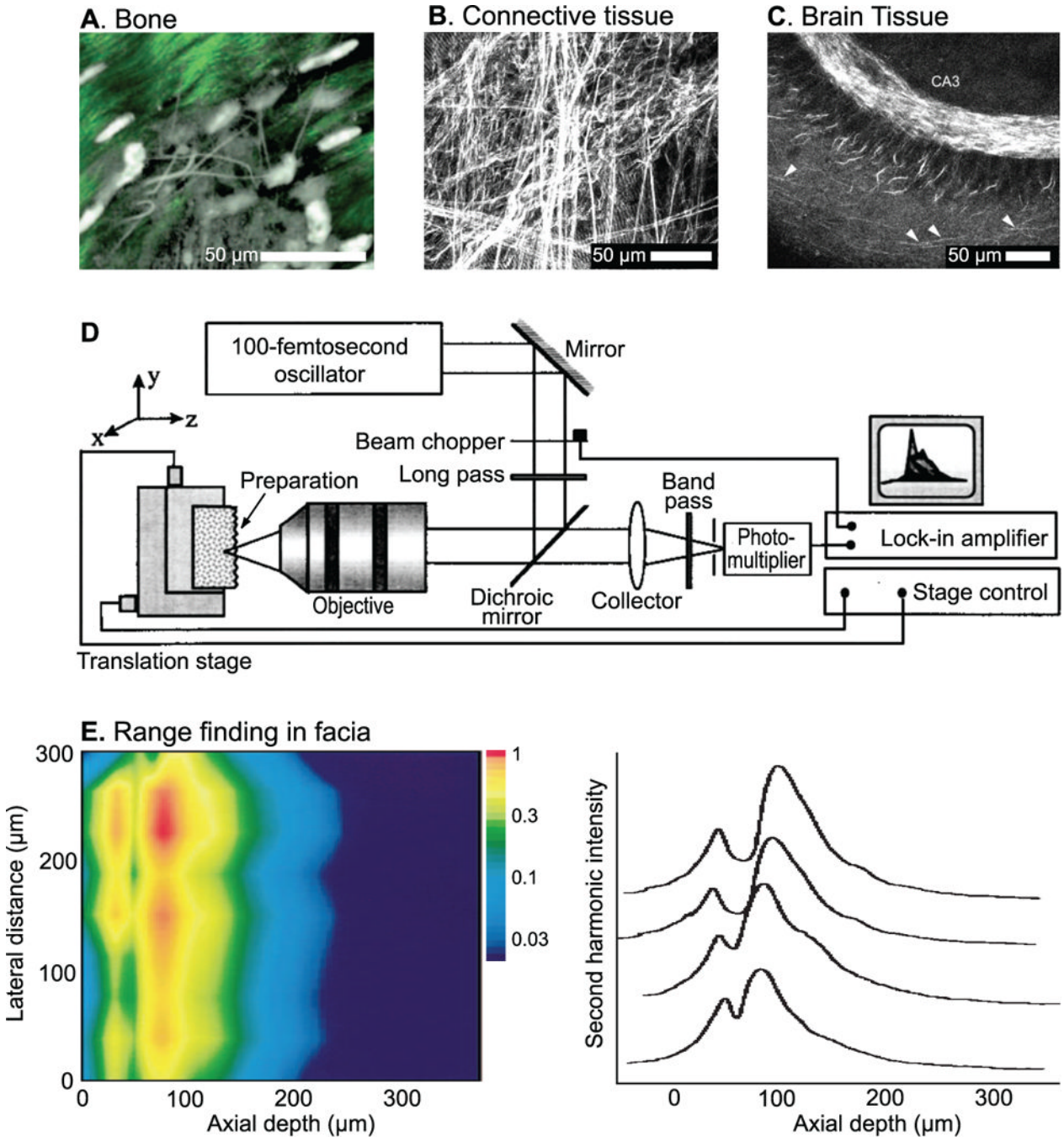

Figure 4. Second harmonic generation from biological tissue using pulsed laser light at amplitudes below the threshold for ablation

(A) The signal from collagenous periosteum (green) and calcein-loaded osteoblast precursors (grayscale) in mouse long bone. Second harmonic light was measured in backscatter. Adapted from [58]. **(B)** Signal from connective and muscle tissue from an explanted leg muscle. Adapted from [60]. **(C)** The signal from the CA3 region *of hippocampus s* hows individual axons that emanate from the pyramidal neurons (arrowheads). Adapted from [61]. **(D)** Schematic of the apparatus for range-finding with second harmonic generation. Adapted from [55]. **(E)** A depth image of a fascia membrane attached to chicken muscle tissue formed from the intensity of the backscattered second

harmonic signal; the logarithm of the signal is shown versus a lateral dimension and depth. The analog values of the depth profile are shown for four lateral positions on the right. Adapted from [55].

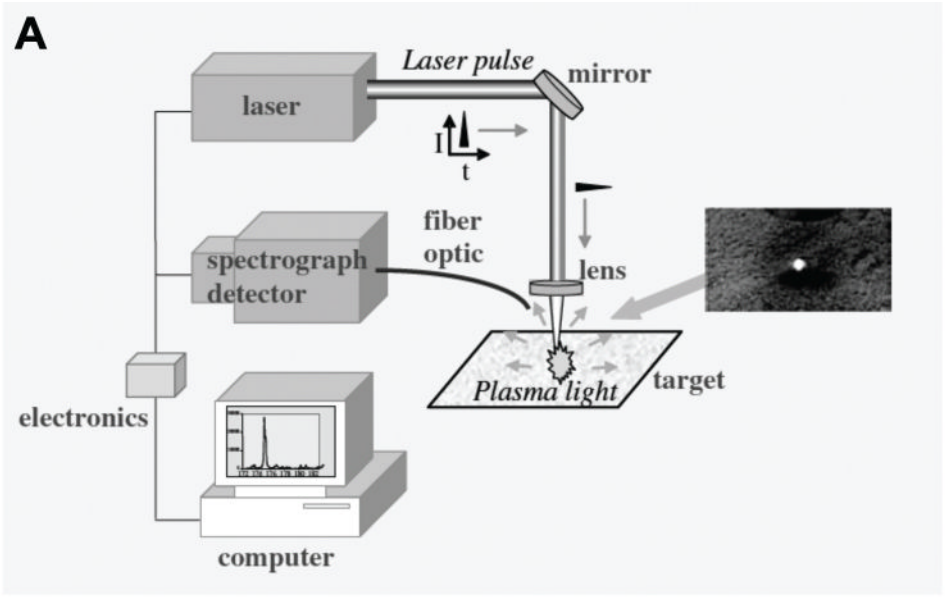

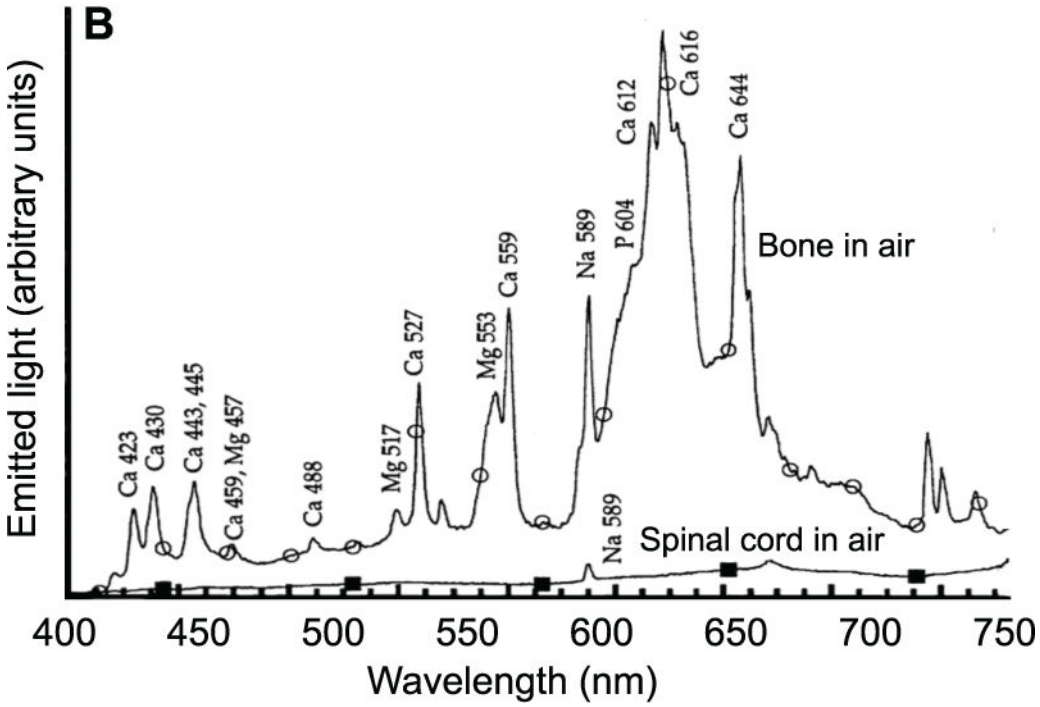

Figure 5. Laser induced plasma spectroscopy using ultra-short laser pulses in air

(A) Schematic of the process. Adapted from [75]. **(B)** The resultant emission spectrum for bone tissue versus spinal cord, a soft tissue. Adapter from [81]. Note that soft tissue only has the sodium D line at 589 nm.

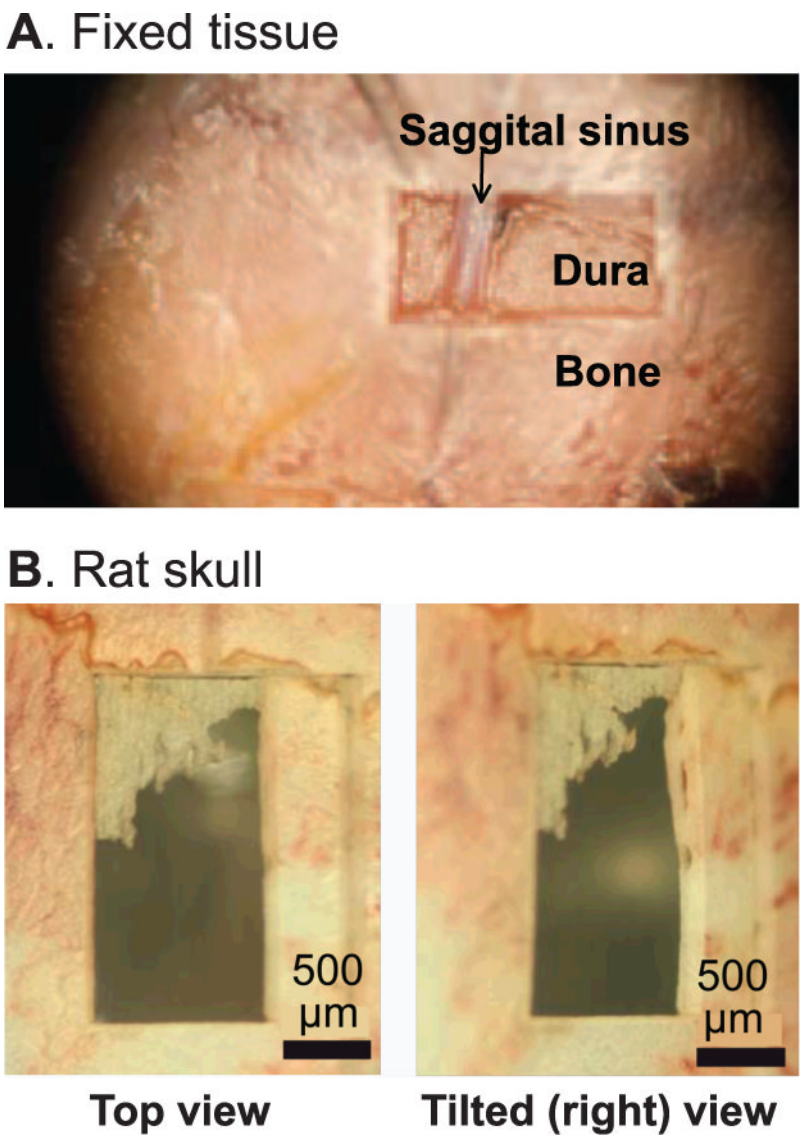

Figure 6. Preliminary results on plasma-mediated ablation of the rodent skull

(A) Data from a fixed but intact animal. **(B)** The use of temporal focusing to achieve a greater depth profile with more efficient cutting. Adapted from [102].